

Models of rotating massive stars: impacts of various prescriptions

Georges Meynet, Sylvia Ekstrom, André Maeder, Patrick Eggenberger, Hideyuki Saio, Vincent Chomienne, Lionel Haemmerlé

Abstract The rotation of stars has many interesting and important consequences for the photometric and chemical evolution of galaxies. Many of the predictions of models of stellar rotation are now compared with observations of surface abundances and velocities, with interferometric studies of fast rotating stars, with internal rotation profiles as they can be deduced by asteroseismology, to cite just a few observational constraints. In this paper, we investigate how the outputs of models depend on the prescriptions used for the diffusion coefficients included in the shellular rotating models. After recalling the various prescriptions found in the literature, we discuss their impacts on the evolutionary tracks and lifetimes of the Main-Sequence (MS) phase, the changes of the surface composition and velocities during the MS phase, the distribution of the core helium lifetime in the blue and the red part of the HR diagram, the extensions of the blue loops, the evolution of the angular momentum of the core, and the synthesis of primary nitrogen in fast-rotating metal-poor

Georges Meynet
Geneva Observatory, Geneva University, CH-1290 Versoix, Switzerland
e-mail: georges.meynet@unige.ch

Sylvia Ekstrom
Geneva Observatory, *ibid.* e-mail: Sylvia.Ekstrom@unige.ch

André Maeder
Geneva Observatory, *ibid.* e-mail: André.Maeder@unige.ch

Patrick Eggenberger
Geneva Observatory, *ibid.* e-mail: Patrick.Eggenberger@unige.ch

Hideyuki Saio
Astronomical Institute, Graduate School of Science, Tohoku University, Sendai 980-8578, Japan
e-mail: saio@astr.tohoku.ac.jp

Vincent Chomienne
Geneva Observatory, *ibid.* e-mail: Vincent.Chomienne@unige.ch

Lionel Haemmerlé
Geneva Observatory, *ibid.* e-mail: Lionel.Haemmerle@unige.ch

massive stars. While some of these outputs depend only slightly on the prescriptions used (for instance, the evolution of the surface velocities), most of them show a significant dependence. The models which best fit the changes of the surface abundances are those computed with the vertical shear diffusion coefficient of Maeder (1997) and the horizontal shear diffusion coefficient by Zahn (1992).

1 Rotation in stellar models

In recent years, many effects of axial rotation on the structure and the evolution of massive stars have been studied (see e.g. the recent review by Maeder & Meynet 2012). Among the effects which are the most important are those linked to the transport of angular momentum and of chemical species in the interior of stars. These may strongly affect many outputs of stellar models such as the variation with the age of the surface abundances and velocities, the evolutionary tracks and lifetimes, the nature of the supernova events and of the stellar remnants, and the nature and the amount of new synthesized species. As a consequence, when results of rotating models are used in population synthesis models or in models for the chemical evolution of galaxies, quite different results are obtained with respect to results obtained from non-rotating models.

Most, if not all of the recent grids of rotating models have been computed in the framework of the theory proposed by Zahn (1992), with further improvements by Maeder & Zahn (1998). This was named the theory of shellular rotation, since it is based on the assumption that on an isobaric surface, the angular velocity, Ω , is nearly constant, that means that any variations can be considered as a small perturbation. This nearly constant value of Ω on an isobaric surface is due to the fact that along those directions, there are neither stable temperature nor density gradients which counteract shear turbulence. This implies the existence of strong “horizontal” (i. e. along an isobaric surface) diffusion coefficient called D_h hereafter. In the following, when we speak about rotating models, we implicitly assume that we consider models with shellular rotation. The present models do not include the effects of the dynamo theory suggested by Spruit (2002)¹.

In the framework of the shellular theory of rotation, the equation describing the transport of chemical species is a pure diffusive equation (Chaboyer & Zahn 1992) written

$$\rho \frac{\partial X_i}{\partial t} \Big|_{M_r} = \frac{1}{r^2} \frac{\partial}{\partial r} \left(\rho r^2 D_{\text{chem}} \frac{\partial X_i}{\partial r} \right), \quad (1)$$

where X_i is the abundance in mass fraction of particles i , and D_{chem} , the appropriate diffusion coefficient for chemical elements (see below).

¹ Numerical simulations by Zahn et al. (2007) have studied MHD instabilities arising in the radiation zone of a differentially rotating star, in which a poloidal field of fossil origin is sheared into a toroidal field. Their simulations show no sign of dynamo action.

In a differentially rotating star, the evolution of the angular velocity Ω has to be followed at each level r (for shellular rotation), so that a full description of $\Omega(r, t)$ is available. The values of $\Omega(r, t)$ influence the mixing of elements and in turn the evolution of $\Omega(r, t)$ also depends on the mixing processes and on the distribution of the elements. The derivation of the equation for the transport of angular momentum is not straightforward. In the case of shellular rotation, the equation in the Lagrangian form becomes (Zahn 1992; Maeder 2009)

$$\rho \frac{\partial}{\partial t} (r^2 \bar{\Omega})_{M_r} = \frac{1}{5r^2} \frac{\partial}{\partial r} (\rho r^4 \bar{\Omega} U_2(r)) + \frac{1}{r^2} \frac{\partial}{\partial r} \left(\rho D_{\text{ang}} r^4 \frac{\partial \bar{\Omega}}{\partial r} \right). \quad (2)$$

Here, $\bar{\Omega}$ is the average value of Ω on an isobar. U_2 is the radial component of the meridional circulation velocity, and D_{ang} , the appropriate diffusion coefficient for angular momentum. The second term on the right is a diffusion term, similar in its form to (1), while the first term on the right is *an advective term*, i. e. modeling the transport by a velocity current. We notice that Eq. (1) does not contain such an advective term. It could contain a term of that kind, however it can be shown (Chaboyer & Zahn 1992) that the combined effect of turbulence and circulation currents is equivalent to a diffusion *for the element transport* (see Eq. 1).

In the equation for the transport of chemical species in radiative zones, the diffusion coefficient, D_{chem} , is made up of two terms. These are the vertical shear diffusion coefficient D_{shear} and the effective diffusion coefficient, D_{eff} , which account for the resultant effect of the strong horizontal shear diffusion, D_{h} (i. e. the shear on an isobaric surface), and of the meridional currents.

In the equation for the transport of angular momentum, the diffusion coefficient, D_{ang} , is made up of only one term, the shear diffusion coefficient D_{shear} .

For the coefficients D_{shear} , we can find two different expressions in the literature.

D_{shear} from Maeder (1997, M97)

$$D_{\text{shear}} = f_{\text{energ}} \frac{H_P}{g\delta} \frac{K}{\left[\frac{\varphi}{\delta} \nabla_{\mu} + (\nabla_{\text{ad}} - \nabla_{\text{rad}}) \right]} \left(\frac{9\pi}{32} \Omega \frac{d \ln \Omega}{d \ln r} \right)^2 \quad (3)$$

where $K = \frac{4ac}{3\kappa} \frac{T^4 \nabla_{\text{ad}}}{\rho P \delta}$, and with $f_{\text{energ}} = 1$, and $\varphi = \left(\frac{d \ln \rho}{d \ln \mu} \right)_{P,T} = 1$.

D_{shear} from Talon & Zahn (1997, TZ97)

$$D_{\text{shear}} = f_{\text{energ}} \frac{H_P}{g\delta} \frac{(K + D_{\text{h}})}{\left[\frac{\varphi}{\delta} \nabla_{\mu} \left(1 + \frac{K}{D_{\text{h}}} \right) + (\nabla_{\text{ad}} - \nabla_{\text{rad}}) \right]} \left(\frac{9\pi}{32} \Omega \frac{d \ln \Omega}{d \ln r} \right)^2 \quad (4)$$

with K , f_{energ} , and φ as in (1).

For the coefficients D_{h} , we can find three different expressions in the literature:

D_{h} from Zahn (1992, Z92)

$$D_h = \frac{1}{c_h} r |2V(r) - \alpha U(r)| \quad (5)$$

where $\alpha = \frac{1}{2} \frac{d \ln(r^2 \bar{\Omega})}{d \ln r}$ and $c_h = 1$.

D_h from Maeder (2003, M03)

$$D_h = A r (r \bar{\Omega}(r) V |2V - \alpha U|)^{1/3} \quad (6)$$

with α as in Eq. (5) and $A = 0.002$.

D_h from Mathis et al. (2004, MZ04)

$$D_h = \left(\frac{\beta}{10} \right)^{1/2} (r^2 \bar{\Omega})^{1/2} (r |2V - \alpha U|)^{1/2} \quad (7)$$

with α as in Eq. (5) and $\beta = 1.5 \cdot 10^{-6}$.

All prescriptions use the same effective mixing coefficient for the chemical species:

$$D_{\text{eff}} = \frac{1}{30} \frac{|r U(r)|^2}{D_h}. \quad (8)$$

There are therefore 6 different combinations of the two shear diffusion coefficients and of the three horizontal diffusion coefficients. The physics sustaining the different expressions for these various diffusion coefficients is described in details in the papers indicated above and we shall not recall them in the present work. We just summarize below a few facts which are useful to keep in mind in order to understand their different impacts in stellar models.

- Since the angular momentum is transported mainly by the meridional currents, one can expect that changing the expressions for the diffusion coefficients will have only a weak impact on the angular momentum distribution in stars. We shall see that this is well verified by the numerical models.
- The diffusion coefficient D_{eff} is the key quantity determining the efficiency of mixing in regions where there is a strong μ -gradient, for instance at the border of the H-convective core.
- The larger D_h is, the smaller will be D_{eff} , and thus less mixing will occur in regions of strong μ -gradients. The expressions of M03 and MZ04 for D_h are larger than the expression given by Z92.
- The diffusion coefficient D_{shear} is the key quantity determining the efficiency of mixing in regions with weak or no μ -gradients, typically in the radiative envelope of massive stars above the H-convective core.
- The two expressions of D_{shear} are strictly equivalent in zones with no μ -gradients.
- The ratio $D_{\text{shear}}(\text{M97})/D_{\text{shear}}(\text{TZ97}) \sim K/D_h$ in regions where $\frac{\rho}{8} \nabla_\mu$ is significantly larger than the difference $\nabla_{\text{ad}} - \nabla_{\text{rad}}$. Since D_h is inferior to K , one has that $D_{\text{shear}}(\text{M97}) > D_{\text{shear}}(\text{TZ97})$.

2 The models computed

In the present work, we study the implications of these different choices on the following model outputs:

- Evolutionary tracks and lifetimes during the Main-Sequence (MS) phase.
- Changes of the surface composition during the MS phase.
- Changes of the surface velocities during the MS phase.
- The distribution of the core helium lifetime in the blue and the red part of the HR diagram.
- The extensions of the blue loops.
- The evolution of the angular momentum of the core.
- The synthesis of primary nitrogen in fast rotating metal poor massive stars.

For that purpose we have computed models for different initial masses, metallicities, rotations with each one of the 6 possible combinations of values for $(D_{\text{shear}}, D_{\text{h}})$ (see Table 1). For each mass and metallicity, the models are labeled by one digit and one letter: 1 is for models computed with the shear diffusion coefficient of Maeder (1997), and 2 for models computed with the shear diffusion coefficient of Talon & Zahn (1997), the letters A, B and C are respectively for the horizontal diffusion coefficient from Zahn (1992), Maeder (2003) and Mathis et al. (2004).

In Table 1, the first column gives the prescription used. The time-averaged equatorial velocity during the MS phase is given in column 2, the MS lifetime is given in column 3, the difference between the surface helium abundance in mass fraction at the end of the MS phase and on the ZAMS is given in column 4. Column 5 presents the N/H ratio obtained at the surface, at the end of the MS phase, and normalized to the initial N/H value. The core He-burning lifetime, and the analogs of columns 4 and 5 but at the end of the core He-burning phase are indicated in columns 6, 7 and 8 respectively. The duration of the core He-burning phase spent in the red ($\log T_{\text{eff}} < 3.68$), in the blue ($\log T_{\text{eff}} > 3.87$) and in the yellow part ($3.68 < \log T_{\text{eff}} < 3.87$) of the HR diagram are given in columns 9, 10 and 11 respectively. The ratio of the time spent in the blue to that spent in the red is shown in column 12, the masses of the helium cores, of the carbon-oxygen cores and of the remnants are given in columns 13, 14 and 15. The mass of nitrogen produced divided by the mass of CNO elements initially present is given in column 16.

3 Evolutionary tracks and lifetimes during the Main-Sequence phase

Figure 1 presents the tracks in the Hertzsprung-Russell diagram (left panel) and the variation of the mass fraction of hydrogen as a function of the Lagrangian mass coordinate (right panel) for the $15 M_{\odot}$ at $Z=0.002$ and with $\Omega_{\text{ini}}/\Omega_{\text{crit}} = 0.5$. One can classify the models in three categories:

Table 1 Models computed in the present work

\bar{v}_{eq} km s ⁻¹	t_{H} My	ΔY_s	$\frac{[N/H]}{(N/H)_{\text{ini}}}$	t_{He} My	ΔY_s	$\frac{[N/H]}{(N/H)_{\text{ini}}}$	t_{blue} My	t_{red} My	t_{yel} My	$\frac{t_{\text{blue}}}{t_{\text{red}}}$	M _{He} M _⊙	M _{CO} M _⊙	M _{rem} M _⊙	$\frac{M(^{14}\text{N})}{M(\text{CNO})_{\text{ini}}}$	
9 M _⊙ , Z=0.002, $v_{\text{ini}}/v_{\text{crit}} = 0.5$															
1A	177	30.065	+0.0149	4.9	2.966	0.0157	4.9	3.0964	0.0970	0.0104	31.9	2.9	1.5	1.3	0.5
1B	-0.6%	-11.8%	+0.0051	3.8	+37.6%	0.0055	3.8	+37.5%	+21.0%	+27.9%	36.3	2.7	1.5	1.3	0.5
1C	+0.6%	-13.3%	+0.0024	3.1	+28.9%	0.0064	3.8	+28.6%	+63.1%	× 2	25.2	2.5	1.4	1.2	0.5
2A	-1.1%	+0.3%	+0.0004	2.2	-11.7%	0.0123	3.5	-52.4%	× 11.1	× 27.3	1.4	2.9	1.5	1.3	0.4
2B	-2.2%	-11.7%	+0.0003	3.0	+17.4%	0.0040	4.2	-10.4%	× 9.6	× 8.7	3	2.6	1.4	1.2	0.9
2C	+0.6%	-13.3%	+0.0017	3.4	+37.1%	0.0099	4.8	+27.7%	× 3.8	× 3.3	10.8	2.5	1.6	1.3	0.4
9 M _⊙ , Z=0.014, $v_{\text{ini}}/v_{\text{crit}} = 0.5$															
1A	163	31.423	+0.0050	2.5	3.291	0.0620	5.8	1.3982	2.0974	0.0997	0.7	2.5	1.4	1.2	0.4
1B	-1.2%	-13.0%	+0.0009	1.8	+47.6%	0.0363	4.9	+64.0%	+35.1%	-14.0%	0.8	1.6	1.4	1.2	0.3
1C	-0.6%	-14.7%	+0.0003	1.6	+36.1%	0.0314	4.7	+53.8%	+27.2%	-18.7%	0.8	1.4	1.2	1.1	0.4
2A	-0.6%	-0.2%	+0.0001	1.3	-5.3%	0.0495	4.5	-42.9%	+12.5%	× 2.1	0.3	2.5	1.4	1.2	0.3
2B	-1.8%	-12.9%	+0.0000	1.6	+17.5%	0.0240	4.2	× $\frac{1}{9.2}$	× 2.0	0.0	0.04	1.7	1.1	1.1	0.4
2C	-0.6%	-14.7%	+0.0002	1.7	+36.8%	0.0242	4.7	× $\frac{1}{8.8}$	× 2.3	× $\frac{1}{14.4}$	0.03	1.5	1.3	1.2	0.3
15 M _⊙ , Z=0.002, $v_{\text{ini}}/v_{\text{crit}} = 0.5$															
1A	197	13.173	+0.0248	5.4	1.323	0.0612	6.9	1.2622	0.0749	0.0416	16.9	5.3	3.0	1.7	0.4
1B	-3.0%	-2.2%	+0.0215	5.1	+8.8%	0.0237	7.1	+18.6%	0.0	× $\frac{1}{3.3}$	-	4.8	2.8	1.6	0.5
1C	-2.5%	-5.3%	+0.0105	4.2	+12.9%	0.0496	5.9	+24.6%	0.0	0.0	-	4.5	2.6	1.6	0.5
2A	-0.5%	-0.4%	+0.0012	2.4	-17.5%	0.0549	5.8	× $\frac{1}{34.2}$	× 4.5	× $\frac{1}{3.7}$	0.03	5.8	3.6	1.8	0.4
2B	-3.0%	-11.5%	+0.0006	3.1	+1.8%	0.0110	4.3	+6.3%	-35.1%	× $\frac{1}{2.0}$	27.6	4.9	2.8	1.6	0.4
2C	-1.5%	-13.5%	+0.0039	3.9	+43.9%	0.0047	4.0	+53.9%	× $\frac{1}{8.6}$	× $\frac{1}{3.6}$	167.5	4.6	3.4	1.8	0.4
40 M _⊙ , Z=0.00001, $v_{\text{ini}}/v_{\text{crit}} = 0.75$															
1A	702	5.559	+0.0949	47.9	0.409	0.0964	48.2	0.4161	0.0	0.0	-	17.1	14.0	4.3	1.1
1B	-2.4%	-2.6%	+0.0743	44.2	+5.7%	0.0753	44.4	+6.0%	0.0	0.0	-	16.7	12.8	4.1	15.3
2A	-2.8%	+1.4%	+0.0459	30.7	-2.5%	0.2006	50.9	-20.8%	0.0	0.0748	-	23.9	17.3	5.3	8.2
2B	-5.3%	-7.4%	+0.0162	27.1	> 5.2%	0.0164	27.2	+4.8%	0.0	0.0	-	20.9	12.9	4.1	105.8

1. The models which present very little differences with respect to the non-rotating model. These are the models 2B (not shown in Fig. 1) and 2C.
2. The models which become overluminous with respect to the non-rotating model but present no significant extension towards lower effective temperatures. These are the models 1A, 1B (not shown) and 1C.
3. Only one model, the model 2A, becomes overluminous and reaches lower effective temperatures at the end of the MS phase.

This behavior reflects differences in the efficiency of mixing in different regions of the stars. The models which are of the less efficiently mixed stars (2B and 2C, due to large D_{h} and thus small D_{eff}) show indeed very little difference in their non-rotating tracks (compare lines for the model 2C and the non-rotating model in Fig. 1). The model 2A presents a situation where there is an efficient mixing at the border of the convective core but where the shear is not so efficient in the radiative envelope. Thus the surface abundances are not yet modified at the stage represented in Fig. 1 (right panel). The larger core increases the luminosity and also is responsible for the extension towards lower temperature of the MS band in the HR diagram (an effect similar to an extension of the core produced by an overshoot). Finally the model which presents the greatest efficiency of mixing both at the border of the

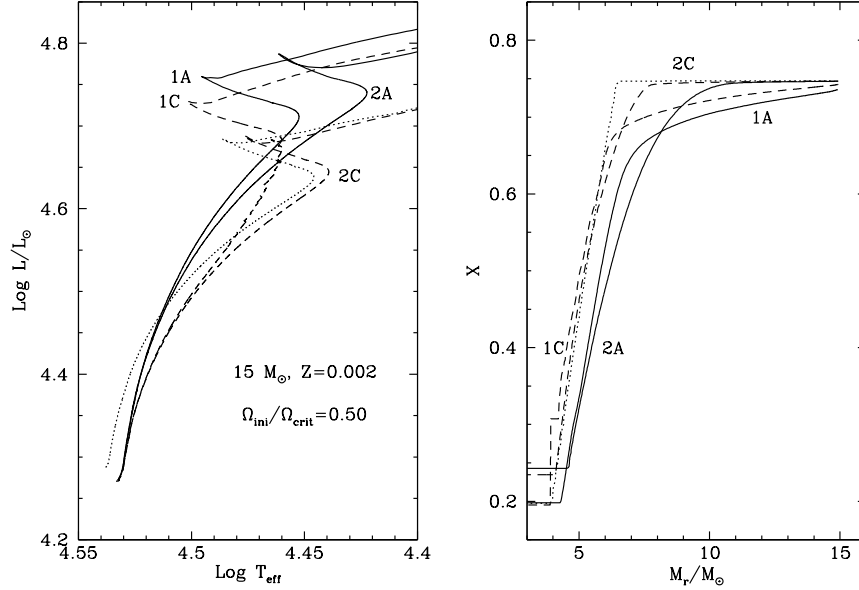


Fig. 1 Evolutionary tracks in the Hertzsprung-Russell diagram (left panel) and the variation of the mass fraction of hydrogen as a function of the Lagrangian mass coordinate (right panel) for the $15 M_{\odot}$ at $Z=0.002$ and with $\Omega_{\text{ini}}/\Omega_{\text{crit}} = 0.5$. The dotted line corresponds to the non-rotating model, the other models are labeled as indicated in Table 1. The models used in the right panel have all a $\log T_{\text{eff}}$ equal to 4.48. The central hydrogen mass fraction is equal to 0.1973 (non rotating model), 0.1982 (1A), 0.2068 (1C), 0.2427 (2A), 0.2244 (2C). The models 1B and 2B are not shown since they present many similarities with the models 1C and 2C.

core and in the radiative zone is the model 1A. This mixing keeps this model in bluer positions in the HR diagram compared to model 2.

One notes that in model 1A, the μ -gradient (with respect to mass) is steeper than in the model 2A, while both models have the same expression for D_{eff} (since they have the same expression for D_{h}). This is because in model 1A, which has D_{shear} larger than in 2A, hydrogen flows more efficiently inwards and helium outwards. This replenishes hydrogen at the border of the core. The net effect of these diffusions of hydrogen and helium is to make the star more luminous and bluer. The same occurs in the 1C model, although the effect is less marked because of the smaller value for D_{eff} .

In Table 1, the MS lifetimes are indicated in column 3. The first row for each model gives the value of the MS lifetime in million years for the model 1A. The rows for the other models show the differences in percentage with respect to the value obtained for the model 1A. We see that the impact on the MS lifetimes remains modest (at most 13.5% for the $15 M_{\odot}$ models considered here) with respect to the precision with which an age estimated can be made through the fitting of an isochrone in this mass domain. On the other hand the scatter is not negligible with respect to the amplitude of the effect of the increase of the MS lifetime due to ro-

tation. Indeed, the increase of the MS lifetime with respect to the non-rotating case amounts to 18.5% for the $15 M_{\odot}$ model.

All the models computed here account for the same overshoot, but Fig. 1 shows that the track will present quite different extensions due to the various prescriptions. One sees also that the models 1A and 2A (those computed with the smaller D_h and thus greater D_{eff}) are the only ones presenting an extension of the core with respect to the non-rotating model. Therefore only the use of these two prescriptions can attribute part of the extension of the convective core to an effect of rotational mixing. Let us note that the recent determination of the extension of the mixed core in fast rotating stars by Neiner et al. (2012) seem to support the view that rotation enlarges the convective core. This would support prescriptions 1A or 2A. In that case, one should use slowly rotating stars in order to constrain the extension of the core due to the process of convective penetration alone as is done, for instance, in Ekström et al. (2012).

4 Changes of the surface composition during the MS phase

The changes of the surface composition during the MS phases can be seen in Table 1 and in Fig. 2 for the $15 M_{\odot}$ at $Z=0.002$ and $\Omega_{\text{ini}}/\Omega_{\text{crit}} = 0.5$ cases. Column 3 and 4 of Table 1 give, at the end of the MS phase, the excesses of helium at the surface of the star (in mass fraction and with respect to the initial value) and the ratio of nitrogen to hydrogen normalized to the initial value, respectively.

Independent of the prescriptions used, one notes, as was already obtained in previous works (see Maeder & Meynet 2001) that the surface enrichment in nitrogen increases in increasing initial stellar masses and that it also increases for decreasing metallicity, in both cases keeping the initial rotation the same and comparing stars at similar evolutionary stages.

One sees also that the surface enrichments are higher when D_{shear} is higher (compare models of series 1 with models of series 2). This is quite logical since D_{shear} is the parameter which governs the transport of chemical elements in the region extending from the vicinity of the core up to the surface.

The greatest surface enrichments are always obtained for the model 1A, the smallest for the model 2A (except for the very metal poor $40 M_{\odot}$ model, but the difference between models 2A and 2B is quite small). For a given model, the variation of the prescriptions used produces a scatter of the N/H value obtained at the end of the MS phase of around a factor of 2. For the excesses in helium, the factors are greater, however, except for the $40 M_{\odot}$ at $Z=0.00001$ case, the enhancements are very modest and well below those which could be estimated from observed spectra.

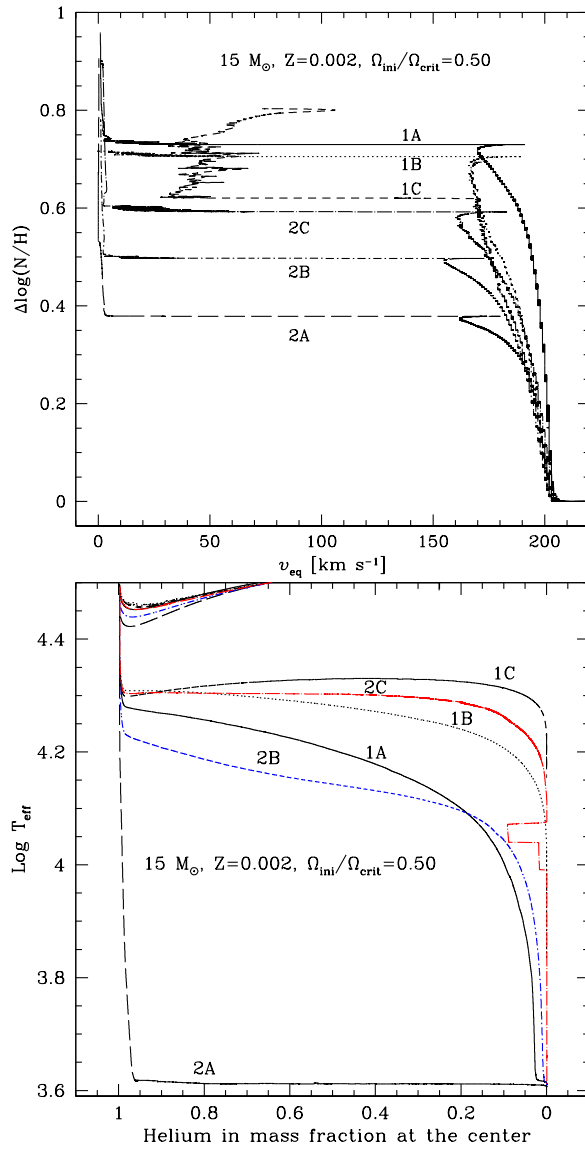


Fig. 2 *Upper panel* Evolution of the N/H ratio at the surface of stellar models computed with various diffusive coefficients as a function of the equatorial velocity. *Lower panel* Evolution of the effective temperature during the core He-burning phases for different prescriptions of the diffusive coefficients.

5 Changes of the surface velocity during the MS phase

Column 2 in Table 1 compares the time-averaged equatorial velocity during the MS phase. The first row of the table indicates the equatorial surface velocity for model 1A in km s^{-1} . The other lines indicate the difference in percentage with respect to model 1A. One sees that the differences are always less than 5.3%, which is small. This is due to the fact that changing the prescriptions for the diffusion coefficients has only a very weak impact on the velocity of the meridional currents. Thus the transport of the angular momentum which is mainly driven by these currents is almost unaffected by changes of the diffusion coefficients.

This can also be seen in Fig. 2 (left panel), which shows the variation of the nitrogen enhancement with respect to the surface equatorial velocity (tracks on this diagram go from right to left as time proceeds). One sees that during the MS phase, all of the models span the same interval in equatorial velocities. What changes is the surface nitrogen enrichment obtained at the end of the MS phase. In the plane N/H versus v_{eq} , model 1A will produce a steeper relation than model 2A.

If one considers mean values of the ratio N/H for B dwarfs in the Galaxy and in the SMC one obtains enhancement factors between 1.6 and 2.5 for the Galaxy and 3.2 and 6.3 for the SMC (see Table 2 in Maeder & Meynet 2012, and references therein). These mean values should be obtained for stars with an average rotation during the MS phase of around 200 km s^{-1} .

At solar metallicity, the $15 M_{\odot}$ model 1A well reproduces the observed enrichments (Ekström et al. 2012). This is not a surprise, since the value of the parameter f_{energ} in D_{shear} , chosen equal to one, has been selected in order to fit these observed enrichments. With the same value of f_{energ} , the $15 M_{\odot}$ at $Z=0.002$ with an average rotation of 200 km s^{-1} and prescriptions 1A predicts an enhancement factor between 3 and 5.3 in the last third of its MS lifetime, which is in the range of the observed values. In that case, no calibration has been made and the good fit supports this kind of model. The other prescriptions gives too low surface enrichments keeping f_{energ} equal to 1.

We note that a value equal to 1 for f_{energ} implies that we really account for the physics involved into the expression for D_{shear} , which would not be the case if one would have to multiply the expression by a constant much greater or much smaller than one!

6 The distribution of the core helium lifetime in the blue and the red part of the HR diagram

The observed number of blue to red supergiants in clusters at different metallicities is an important feature that stellar models should be able to reproduce. This is important for many reasons, for instance to predict the correct photometric evolution of young starburst regions or the nature of the progenitors of the core collapse su-

pernovae. It happens that observation shows that the blue to red ratio in clusters with masses at the turn off between 9 and 30 M_{\odot} increases when the metallicity increases, while standard stellar models predict that the blue to red supergiant ratio decreases when the metallicity increases (Meylan & Maeder 1982; Langer & Maeder 1995; Eggenberger et al. 2002; Meynet et al. 2011b). The blue to red supergiant ratio has also been discussed in the context of field stellar populations in Hartwick (1970); Dohm-Palmer & Skillman (2002).

At the moment, there is no explanation for this general trend. On the other hands, many works could reproduce the blue to red supergiant ratios observed at one given metallicity by changing the mass loss rates (see e.g. Salasnich et al. 1999) or mixing (Langer & Maeder 1995; Maeder & Meynet 2001). In this paper we shall not discuss all the aspects of this question but focus on the importance of mixing.

Looking at the right panel of Fig. 2, which shows the evolution of the effective temperature during the core Helium burning phase, we see that only one set of diffusion coefficients (the one using the D_{shear} of Talon & Zahn 1997, and the D_{h} of Zahn 1992) makes the 15 M_{\odot} at $Z=0.002$ evolve rapidly to the red part of the HR diagram after the MS phase. This is the prescription that we used in Maeder & Meynet (2001), where we suggested that rotational mixing could help a lot in reproducing the observed blue to red supergiant ratio in the Small Magellanic Cloud. In view of the present results we see that, while this conclusion might always be correct, it is however quite dependent on the prescriptions used for the diffusion coefficients.

It is interesting to identify from the numerical experiments performed in this work, the conditions which favor a rapid redward evolution at low metallicity. It does appear that two conditions have to be satisfied: 1) The mixing at the border of the convective cores (both during the H- and He-burning phases) have to be sufficiently efficient. Indeed, we see that any very strong values for D_{h} , which prevent any strong mixing in regions with strong molecular weight gradient (μ -gradient), also prevents the star evolving to the red phase. 2) The mixing in the zones where the μ -gradients are weak, namely the outer part of the radiative envelope, should not be too strong, because any strong mixing there would make the star be more “homogeneous” and thus maintain a bluer position in the HR diagram. As very often noticed in the literature, we see that this red to blue evolution is a feature which is very sensitive to many physical ingredients of the models. The fact that it depends on subtle changes of the efficiency of mixing in different regions of the star is just one illustration of this.

Taken at face value, the set of diffusion coefficients D_{shear} from Talon & Zahn (1997), and the D_{h} of Zahn (1992) appear as the most favored to explain the blue to red supergiant ratio at low metallicity. However, other parameters — for instance the changes of the surface abundances expected for an averaged rotational velocity — are better fitted with the prescription 1A (keeping $f_{\text{energ}} = 1$). Moreover, since mass loss, both during the MS phase and at the red supergiant phase, plays a key role in shaping the blue to red supergiant ratio (see e.g. the discussion in Meynet et al. 2011b), it may be premature to use the observed variation of the blue to red supergiant ratio to constrain the prescription to be used. Probably in order to make progress in this area of research two important points have first to be settled: 1) to

distinguish, using observations of the surface abundances and/or of the vibrational properties, those blue supergiants which are direct successors of MS stars from those which are on a blue loop after a red supergiant stage. The ability to distinguish, at different metallicities, between those blue supergiants coming from the MS phase from those coming from the red supergiant phase would improve considerably our understanding of the blue supergiant formation process; 2) to obtain more reliable mass loss rates especially during the red and blue supergiant phases.

7 The extensions of the blue loops

Another feature which is sensitive to the form of the diffusion coefficients is the extension of the blue loops for stars with masses between about 3 to 12 M_{\odot} . This is important in order to predict the populations of Cepheids, and also for the blue to red supergiant ratio discussed above, since the presence of a blue loop (when compared with the same model without blue loop) will reduce the lifetime of red supergiant but increase that of the blue supergiant.

Looking at Fig. 3, we can see the following features: at $Z = 0.002$, the duration of the blue loops increases more and more passing from models 2A, to 2B, and then to 2C. When the D_{shear} is changed (model 1), the “loop” (if we can still speak of a loop in this case) even begins in the blue part of the HR diagram.

At $Z=0.014$, the situation is quite different, first the loops in all models are significantly reduced, which is a well-known effect when the metallicity increases. Second, models 2B and 2C do not show any loops. In case such prescriptions would be adopted, then only slow rotators can show a blue loop and thus explain the existence of Cepheids. If such prescriptions were to be adopted, then only slow rotators could show blue loops and thus explain the existence of Cepheids.

We can note also that in the first set of models (labels beginning with one, i. e. D_{shear} from Maeder 1997), the impact of changing D_h on blue loops is quite modest in both metallicities. In the second set of models, changing D_h has a strong effect.

At low metallicity, models 2A for 9 M_{\odot} would be the more helpful to reconcile the theoretical predictions with the observations as was suggested from previous section which focused on 15 M_{\odot} stellar models. At solar metallicity, whatever model is considered, the blue to red supergiant ratios do appear too low (at most 1 while it is observed at around 3). At this metallicity, the problem may be at least partially cured by enhancing the mass loss rate during the red supergiant phase.

8 The angular momentum of the core

During the evolution of a star, the core loses some angular momentum, mainly due to the effect of meridional currents. It happens that, in shellular rotating models without interior magnetic field, these losses are not sufficient to explain the rela-

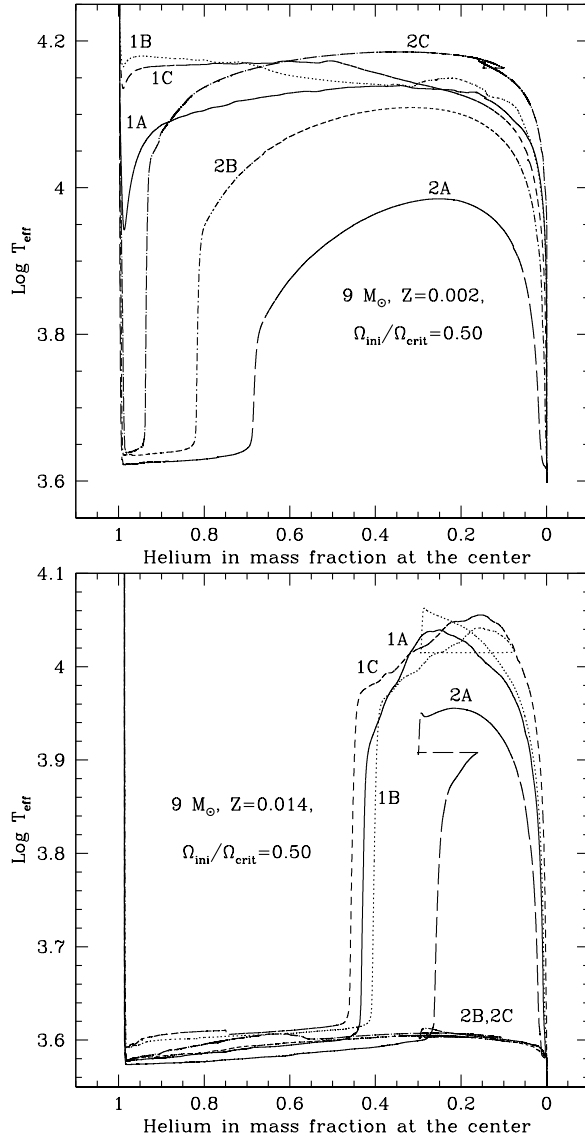


Fig. 3 *Upper panel* Evolution of the effective temperature during the core He-burning phases for different prescriptions of the diffusive coefficients in a rotating $9 M_{\odot}$ stellar model at $Z=0.002$. *Lower panel* Same as the panel on the left at $Z=0.014$.

tively long observed rotation periods of young pulsars (Heger et al. 2004). This is the reason why some authors have considered much stronger coupling between the core and the envelope by introducing a magnetic field which forces solid body rotation or near solid body rotation during the MS phase (Heger et al. 2005). Here, we have not accounted for such a strong coupling. A question however that we may ask is the extent to which this loss of angular momentum depends on the prescription used. Are there any of these prescriptions which would significantly change the angular momentum contained in the core at the end of its evolution?

A priori, one would expect that the loss of angular momentum by the core due to the transport processes should be only slightly dependent on the various prescriptions because, as already stressed, during most of the stellar lifetime, angular momentum is transported by the meridional currents whose velocities are only weakly dependent on the choice of D_h . Let us, however, check this point in the numerical models that we have. Since we have not pursued the computation beyond the end of the core He-burning phase, we compare here the angular momentum of the core obtained at the end of the core helium burning phase. The masses of the remnant of the different $15 M_\odot$ $Z=0.002$ models are between 1.6 and $1.8 M_\odot$. The angular momentum which would be locked into the $1.6 M_\odot$ remnant supposing that no change does occur in the advanced phases of the evolution, would be between 0.93 and $1.14 \cdot 10^{50} \text{ g cm}^2 \text{ s}^{-1}$ depending on the prescription used. The analog values in the case that the remnant is $1.8 M_\odot$ would be between 1.19 and $1.44 \cdot 10^{50} \text{ g cm}^2 \text{ s}^{-1}$. So we see that these quantities present a scatter around their mean values of at most 20%.

Is such a scatter important? As it concerns the missing angular momentum loss of the core, the answer is clearly no. To illustrate this, let us derive the following numerical estimate: if we lock an angular momentum content of $1 \cdot 10^{50} \text{ g cm}^2 \text{ s}^{-1}$ in a neutron star, it would show a rotation period of about 0.1 ms , smaller by a factor between 4 and 7 than the critical periods for neutron stars which are between 0.44 and 0.65 ms as given by Georgy et al. (2012). The period is also smaller by two to three orders of magnitude than the observed periods of young pulsars which are between 20 and 100 ms (Muslimov & Page 1996; Marshall et al. 1998). We can at least conclude that the missing transport mechanism cannot be due to a particular choice of the diffusion coefficients for D_{shear} and D_h , since whatever choice is made, the angular momentum content of the core is more or less the same at the end of the core He-burning phase.

The angular momentum losses of the core may be underestimated either during the H and He-burning phases of the star and/or in the advanced phases and/or at the time of the supernova explosion and/or during the early years of the evolution of the new born neutron star. It may be that magnetic braking may play a role in this context (Meynet et al. 2011a).

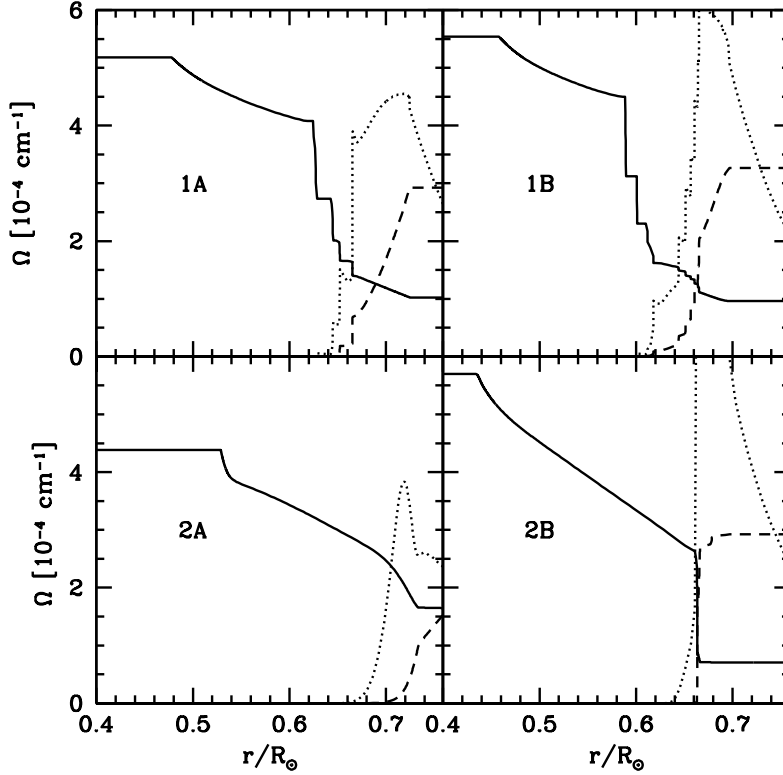


Fig. 4 Variation of the angular velocity as a function of the radius inside the $40 M_{\odot}$ stellar models when the mass fraction of helium at the center is equal to 0.45. The dotted lines show, in each model, the variation as a function of the radius of the rate of production of energy by H-burning, ϵ_{H} , in units of $10^5 \text{ ergs g}^{-1} \text{ s}^{-1}$.

9 The synthesis of primary nitrogen in fast-rotating metal-poor massive stars

Fast-rotating massive stars may be the sources of primary nitrogen in the early phases of the evolution of galaxies (Chiappini et al. 2006, 2008). Therefore it is important to assess the extent to which the primary nitrogen production depends on the prescriptions used. In the last column of Table 1, we have indicated the mass of nitrogen (in solar masses) present in the region outside the stellar remnant normalized by the mass of CNO elements that were initially present in the same region of the star. We call this quantity $M(^{14}\text{N})/M(\text{CNO})$. When nitrogen is produced by the transformation of the carbon and oxygen initially present in the star (secondary nitrogen production channel), then the quantity shown in Table 1 can at most be equal to one. It would be one if all the carbon and oxygen initially present in that region were to have been transformed into nitrogen. Actually it is less than one because, in

the regions inside the H-burning shell, the nitrogen which has been produced by the CNO burning will then have been further transformed into ^{22}Ne .

We see that $M(^{14}\text{N})/M(\text{CNO})$ is inferior to one except in the fast-rotating very metal-poor $40 M_{\odot}$ stellar models. This illustrates the results already discussed by Meynet & Maeder (2002); Meynet et al. (2006) that rotational mixing, by bringing carbon and oxygen (freshly synthesized in the helium-burning core) into the H-burning shell, enhances significantly the quantities of nitrogen produced. The quantities produced are no longer limited by the initial metallicity of the star, since the carbon and oxygen transformed into nitrogen are synthesized by the star itself through helium transformation (primary nitrogen production channel).

We see, however, that the enhancements of primary nitrogen production present great variations depending on the prescriptions used for D_{shear} and D_{h} . Before we analyze these results in more detail, let us recall a few general facts:

1. Primary nitrogen production depends on the efficiency of transport mechanisms in the region between the He-burning core and the H-burning shell;
2. The diffusion coefficient which dominates the transport in that region is D_{shear} . A careful reader may be puzzled by such a statement since we mentioned above that D_{shear} operates mainly in weak μ -gradient regions while the appropriate diffusion coefficient in strong μ -gradient regions would be D_{eff} . Does it mean that the μ -gradients are not so strong at the border of the He-burning core? The answer is yes. Indeed, in the core-shell intermediate region, most of the time, the gradients of μ are not very strong since the connected regions are all helium rich, moreover the gradient of Ω which enters into the expression for D_{shear} is important.
3. Since D_{shear} is the dominant diffusion coefficient, the gradient of Ω becomes the key factor for primary nitrogen production, a small gradient producing less efficient shear mixing than a steep gradient.

In Fig. 4, we can see the variations of Ω as a function of the radius in the $40 M_{\odot}$ stellar models when the mass fraction of helium in the core is equal to 0.45 (that means models at the middle of the core He-burning phase). We see that models using the prescription by Maeder (1997) have a smooth gradient immediately above the convective core and show in outer zones a succession of regions with very steep and flat gradients. We shall call this zone the cliff. The cliff corresponds to the transition between the envelope and the core. The H-burning shell is more or less at its base (see Fig. 4).

The smooth gradient results, at least in part, from the activity of the shear transport having occurred during the core He burning phase. The flat Ω regions in the cliff are produced by intermediate convective zones which are no longer present at the stage shown in the figure but have appeared in previous stages of the evolution of the star. In the present models, we assume that convective regions rotate as solid bodies, hence the flattening of Ω in these zones. The flat regions present a very low D_{shear} coefficient since the Ω -gradients are very small. The part of the Ω profile which is important for primary nitrogen production is the portion with a smooth gradient just above the He-burning core.

In the model 1B (higher D_h and thus smaller D_{eff}), we note that the smooth gradient zone is more compact, making the gradient of Ω in that region steeper. This results from the less efficient chemical mixing at the border of the H-burning core. As a result, the helium core will be smaller and the transition zone between the core and the shell in a deeper part of the star. Since model 1B presents a steeper gradient of Ω in the smooth gradient zone, it produces more primary nitrogen than model 1A (see Table 1).

The configurations presented in the bottom panels, resulting from prescriptions 2A and 2B, show different characteristics with respect to models 1A and 1B in upper panels: 1) just above the core the gradient of Ω is steeper; 2) the region with a succession of strong Ω -gradients and flat portions no longer exists. These two features result from less efficient shear transport at the border of the burning cores. Again, as in model 1, we see that when high values of D_h are used, stronger gradients are obtained.

We can see from Table 1 that, actually, the primary nitrogen production is larger in the models 1B, 2A and 2B than in model 1A as can be expected from the line of reasoning above. An interesting conclusion of this discussion is that primary nitrogen production depends mainly of the gradient of Ω just above the helium burning core.

10 Conclusions

We have studied the impact of various prescriptions on important outputs of rotating massive star models. The main conclusions are the following:

- The outputs of stellar models which show marginal dependence on the prescriptions used for D_{shear} and D_h are the MS lifetimes, the evolution of the surface velocities, and the evolution of the angular momentum of the core.
- The outputs of stellar models which show significant dependence on the prescriptions used for D_{shear} and D_h are the shape of the evolutionary tracks, the surface enrichments predicted for a given initial rotation, the blue to red evolution, and the extensions of blue loops and the amount of primary nitrogen produced.
- The general trends of the increase of the mixing efficiency with the increase of the initial mass of the star, of its initial rotation and with the decrease of the initial metallicity remain the same whatever the prescriptions used for D_{shear} and D_h .

The hope would be, of course, to identify the most realistic diffusion coefficients on the basis of physical considerations. From an analytic point of view, the difficulty is mainly in how to treat turbulence. This is reflected by the fact that in each of these expressions, a free parameter is present (f_{energ} in D_{shear} for instance). At the moment this free parameter is chosen so as to allow models to reproduce one well identified observed feature (for instance, the surface enrichments observed at the surface of

MS B-type stars at solar metallicity). Thus a good fit with the observed feature which has been used to calibrate the models is not a test of the models. The tests of the models are comparisons with other observed features such as comparisons with surface enrichments for other velocities, metallicities or initial mass ranges. We show above that prescription 1A can account for the observed enrichments in the SMC, while the prescription has been calibrated on solar metallicity stars. Thus this can be viewed as a support of this kind of model.

We see also that one set of prescriptions cannot give satisfactory fit to all the observed features discussed here. This is expected since these observed features are not all governed only by the way mixing is treated. As indicated in the paper, the blue to red supergiant ratio, for instance, also depends a lot on the way in which the mass loss due to stellar winds is implemented in the models. Moreover, other effects, not accounted for here, such as close binary evolution, or magnetic braking, may also contribute to some of the observed features.

In order to progress on the theoretical side, the key points reside in the capacity to treat turbulence in a more rigorous way. The key to progress on the theoretical front would seem to be the ability to treat turbulence in a more rigorous way. Probably multidimensional hydrodynamical simulations can provide important hints on this topic (Arnett & Meakin 2011).

Another complementary approach is to use well-observed stars to constrain the models. Stellar models which can account for many observed features have a great chance to provide a realistic description of the structure of stars. It may be sometimes for wrong reasons, in the sense that the physical process invoked may not be exactly the one operating in nature, but the effect of this physical process, whatever it is, has some chance to produce the structure as obtained in the model which best fits the observations.

We are confident that improvements in the two directions of hydrodynamical simulations and comparisons of evolutionary models with observed stars will allow us to constrain the possibilities for the physics occurring in stellar interiors.

Acknowledgements The authors thank Dr Kévin Belkacem for the careful copy editing of the manuscript.

References

- Arnett, W. D., & Meakin, C. 2011, *ApJ*, 741, 33
 Chaboyer, B. & Zahn, J.-P. 1992, *A&A*, 253, 173
 Chiappini, C., Ekström, S., Meynet, G., et al. 2008, *A&A*, 479, L9
 Chiappini, C., Hirschi, R., Meynet, G., et al. 2006, *A&A*, 449, L27
 Dohm-Palmer, R. C. & Skillman, E. D. 2002, *AJ*, 123, 1433
 Eggenberger, P., Meynet, G., & Maeder, A. 2002, *A&A*, 386, 576
 Ekström, S., Georgy, C., Eggenberger, P., et al. 2012, *A&A*, 537, A146
 Georgy, C., Ekström, S., Meynet, G., et al. 2012, *ArXiv e-prints*
 Hartwick, F. D. A. 1970, *Astrophys. Lett.*, 7, 151

- Heger, A., Woosley, S. E., Langer, N., & Spruit, H. C. 2004, in IAU Symposium, Vol. 215, Stellar Rotation, ed. A. Maeder & P. Eenens, 591
- Heger, A., Woosley, S. E., & Spruit, H. C. 2005, *ApJ*, 626, 350
- Langer, N. & Maeder, A. 1995, *A&A*, 295, 685
- Maeder, A. 2009, *Physics, Formation and Evolution of Rotating Stars*, ed. A. Maeder
- Maeder, A. & Meynet, G. 2001, *A&A*, 373, 555
- Maeder, A. & Meynet, G. 2012, *Reviews of Modern Physics*, 84, 25
- Maeder, A. & Zahn, J.-P. 1998, *A&A*, 334, 1000
- Marshall, F. E., Gotthelf, E. V., Zhang, W., Middleditch, J., & Wang, Q. D. 1998, *ApJ*, 499, L179
- Meylan, G. & Maeder, A. 1982, *A&A*, 108, 148
- Meynet, G., Eggenberger, P., & Maeder, A. 2011a, *A&A*, 525, L11+
- Meynet, G., Ekström, S., & Maeder, A. 2006, *A&A*, 447, 623
- Meynet, G., Georgy, C., Hirschi, R., et al. 2011b, *Bulletin de la Societe Royale des Sciences de Liege*, 80, 266
- Meynet, G. & Maeder, A. 2002, *A&A*, 390, 561
- Muslimov, A. & Page, D. 1996, *ApJ*, 458, 347
- Neiner, C., Mathis, S., Saio, H., et al. 2012, *A&A*, 539, A90
- Salasnich, B., Bressan, A., & Chiosi, C. 1999, *A&A*, 342, 131
- Spruit, H. C. 2002, *A&A*, 381, 923
- Zahn, J.-P. 1992, *A&A*, 265, 115
- Zahn, J.-P., Brun, A. S., & Mathis, S. 2007, *A&A*, 474, 145